**Noname manuscript No.**
(will be inserted by the editor)

# Nonlinear tensile behaviour of elementary hemp fibres: A numerical investigation of the relationships between 3D geometry and tensile behaviour

**A. Del Masto · F. Trivaudey · V. Guicheret-Retel · V. Placet · L. Boubakar**

Received: date / Accepted: date

**Abstract** Experimental observations shown that most of plant fibres are characterised by an intricate structure, morphology and organisation. This complex geometrical characteristics may affect the mechanical behaviour of this kind of natural fibres and contribute to the high variability of their mechanical properties. So, this study proposes a numerical investigation on the relationship between the cross-section shape of primary hemp bast fibres and their tensile behaviour. A 3D viscoelastic model based on finite element method is used for this study. Real and elliptical simplified cross-section shapes are considered. Results of the tensile test simulations clearly show the strong influence of the degree of ellipticity on the tensile response of the fibre, and more exactly on the shape of the non-linearity of the response. Results also show that this morphologic effect is strongly related and coupled to structural parameters and physical mechanisms, such as the cellulose microfibrils angle and the viscoelastic behaviour of the material of the fibre wall. Geometric issues could then contribute to explain the different types of tensile behaviour experimentally observed and deserve to be taken into account in plant fibre models.

**Keywords** Computational modelling · Hemp fibres · Morphology · Mechanical behaviour

## 1 Introduction

Sustainable development issues prompt industrial and academic research to propose high-performance materials that comply with all the new environmental preservation interests. Natural fibres are nowadays good candidates for replacing synthetic man-made fibres in reinforcing organic matrices in high performance

A. Del Masto
Univ. Bourgogne Franche-Comté, FEMTO-ST Institute
CNRS/UFC/ENSMM/UTBM
Department of Applied Mechanics
E-mail: alessandra.del_masto@univ-fcomte.fr
24 rue de l'Epitaphe, 25000 Besançon, France

composite applications. Fibres derived from plants, such as hemp, flax, jute and alfa fibres appear attractive for many industrial applications [1] thanks to their high specific properties, especially compared to those of glass fibres [2]. However, the use of plant fibres in high-performance composite applications still needs much more work to do, especially in the fields of mechanical characterisation, modelling and optimisation of the processing technologies [3]. One of the difficulties lying with plant fibre composites (PFCs) is the complexity of their mechanical behaviour [4–6] exhibiting non-linearity and time dependency. The origins of such complex behaviour is not yet completely understood. To date, it has been reproduced using mainly phenomenological models such as the viscoelastoplastic model proposed by Poilâne et al. [7] for flax/epoxy composite.

Since a non-linear behaviour is also generally observed at the scale of the single fibre [8; 10–12], one of the open issues in the scientific community still remaining to be elucidated is to know if the non-linear behaviour of the unidirectional PFCs may result from that of the single fibres themselves. Many authors have experimentally investigated the non-linear tensile behaviour of different species of plant fibres [10; 13; 14; 16–18] and the variability of their mechanical properties [19; 20; 22–25], particularly in relation to their microstructure. Literature emphazises that hemp fibres exhibit, in particular, three typical kinds of tensile behaviours: 'Type 1' is truly linear, 'Type 2' is non-linear with a decrease in rigidity above a yield point and 'Type 3' presents multiple non-linearities [11; 12]. The latter is generally considered as a typical behaviour of wood and bast fibres. Up to now, this was generally attributed or related to three main parameters:

(a) The initial value of the cellulose microfibrils angle (MFA). Page et al. [26] studied in the 70's the possible origins of the S-shaped behaviour of wood fibres using an experimental approach. They showed that the shape of the non-linear tensile curve strongly depends on the initial cellulose microfibrils angle (MFA) of the fibres.
(b) The variation of MFA along the fibre. The non-linear tensile behaviour of hemp and wood fibres was explained and modelled respectively by Nilsson and Gustafsson [13] and Sedighi Gilani [10] by introducing disclocations in the helical structure of the cellulose fibrils or assuming a non-uniform distribution of cellulose microfibrils along the fibre and considering elasto-dissipative behaviour for amorphous polymers.
(c) The reorientation of the cellulose microfibrils under tensile loading. At last, other authors have attributed this non-linear behaviour to a stick-slip mechanism inside the fibre wall [17; 18].

In a previous work [27], our team proposed a scenario based on several mechanisms including viscoelastic strain, cellulose microfibrils reorientation and shear strain-induced crystallisation of the amorphous paracrystalline components. These mechanisms were then modelled through an anisotropic viscoelastic constitutive law, describing finite tranformations through a material rotating frame formulation [16]. Results showed that this model is able to correctly simulate the shape of the experimentally observed tensile curves. These conclusions were collected considering a perfectly cylindrical geometry for the fibres. The possible variation in cross-section shape and size along the fibre length [28], the non-zero degree of ellipticity (i.e. non-circular cross-sections) and their induced effects on the fibre mechanical behaviour (stress concentration, fibre rotation...) were therefore not

| Fibre dimensions | |
|---|---|
| Fibre diameter | 10 - 50 $\mu m$ |
| Fibre surface | 780 $\mu m^2$ +/- 300 $\mu m^2$ |
| Lumen diameter | 0.5 - 10 $\mu m$ |
| Lumen surface | 72.6 - 130.6 $\mu m^2$ ( 2 - 16 % total surface) |
| Cell wall thickness | 2 - 15 $\mu m$ |

Table 1: Hemp fibre dimensions, data from literature [33], [34], [35].

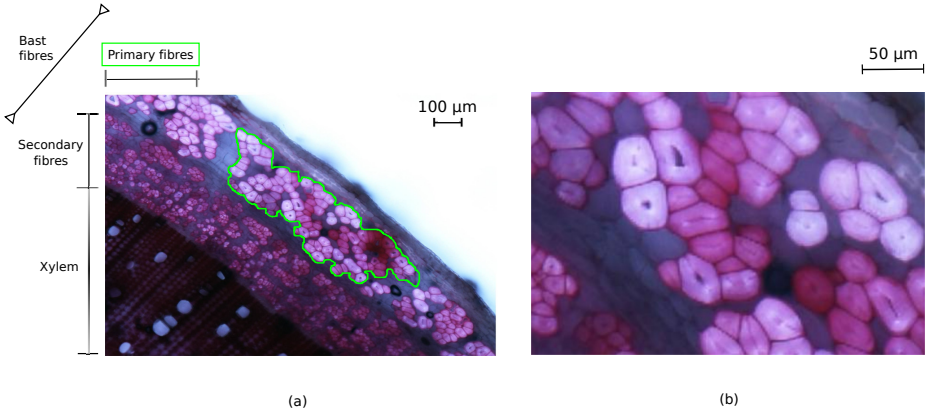


Fig. 1: Hemp stem cross-section (a). Magnification on primary hemp bast fibres (b).

addressed in this previous study. However, experimental observations have clearly shown that most of the plant fibres, including hemp fibres, are characterised by a complex morphology [29; 30]. Their geometry depends on their growing, harvesting and processing conditions and might exhibit large dispersions. These fibres have generally a complex rounded polygonal outer shape which is irregular and non-uniform along length of the fibre and also varies from one fibre to another [31; 32]. The fibre outer diameter generally lies between 10 µm and 50 µm [33]. The central cavity can be narrow, round or elliptical, with a diameter depending of the plant maturity (Fig. 1) lying between 0.5 µm and 10 µm. According to the literature (Table 1), the lumen cross-section area is evaluated between 13% and 16% of the total cross-sectional surface of the fibre. So, it is possible that such geometrical features may have an influence on the mechanical behaviour of plant fibres, in particular on the observed non-linearities of the experimental mechanical responses.

The relationship between the fibre diameter and/or cross-sectional area and its mechanical properties has already been studied for different species, such as hemp [11], [14], flax [36; 37], sisal [8] and stinging nettle [9]. The dependence of the elastic properties is generally attributed to a structural effect [14] and can also originate from a mis-estimation of the cross-sectional area of the fibre [15]. Indeed, its determination is more complex than for solid circular man-made fibres. The description and determination of the 2D and 3D shapes of the plant fibres still

represent a real challenge from an experimental point of view. The difficulty comes generally from the size and fragility of elementary fibres making preparation and handling challenging. Promising results have been recently obtained by Placet et al. [31] on hemp fibres using FIB (Focused Ion Beam) tomography and Optical Coherence Tomography (OCT) and also by Joffre et al. [38] on wood fibres using X-ray microtomography. Some authors have also provided a methodology for the numerical modeling of the scattering observed in the geometry of plant fiber cross-sections [32], [39] using numerical methods. Gassan et al. [40] also pointed out the influence of the shape of the fibre cross-section on the apparent elastic modulus. Using an elastic model based on the thick laminated tube model, they showed that the longitudinal apparent elastic modulus of the fibre is lower for circular cross-section based fibres than for fibres with a cross-section with a high degree of ellipticity. Even if the relationships between the shape of the fibre cross-section and its elastic properties have been widely studied in literature, there remains that, to the best authors' knowledge, no work has studied its possible influence on the shape of the tensile response. So, in this study, we propose to investigate this issue. When compared to purely cylindrical geometry, it is possible that more complex geometries induce effects on the fibre mechanical behaviour including stress concentrations, non-linearities, buckling and mechanical coupling (twist), and, ultimately, on the mechanical behaviour of composites reinforced with such fibres. Due to the difficulties related to the experimental reconstruction of the real 3D fibre morphology, a numerical approach is mostly preferred to investigate the relationship between morphology and the tensile behaviour of isolated elementary plant fibres. In this paper, the model developed by Trivaudey et al. [16] is associated with different 3D geometries of the fibre, in order to evaluate the influence of the morphology on the fibre tensile behaviour. Real and simplified cross-section shapes are considered and a finite elements modelisation is performed.

## 2 Methods and materials

### 2.1 Microscopic observation and image processing of primary hemp bast fibres

Fresh transverse sections were cut from the middle region of hemp stems using a razor blade. A monoeicious hemp (*Cannabis sativa*) variety (*Futura 75*) grown in 2013 was studied. Cytochemical staining of lignin was achieved on sections using the Wiesner reagent (phloroglucinol - HCl) that gives a purple-red coloration to lignin. This coloration helps the definition of the fibre wall outlines (the middle lamella is generally lignin rich). Observations and measurements were performed using an optical microscope (Nikon Eclipse LV150). Recorded images were processed using automatic or manual processing (depending on the quality of the images: contrast, brightness...). Approximately 30 fibres were studied. Their inner and outer contours were extracted and morphologic parameters such as diameters and wall surfaces were determined. The contour lines of the external shape of some fibres and of their lumens were determined using the microscopic optical pictures (Fig. 1) and pattern recognition tools implemented in the Matlab® code. At this point, some classical image filtering techniques were carried out, such as contrast enhancement and Otsu's method threshold (Fig. 2), in order to recognise the contour lines of the fibres section.

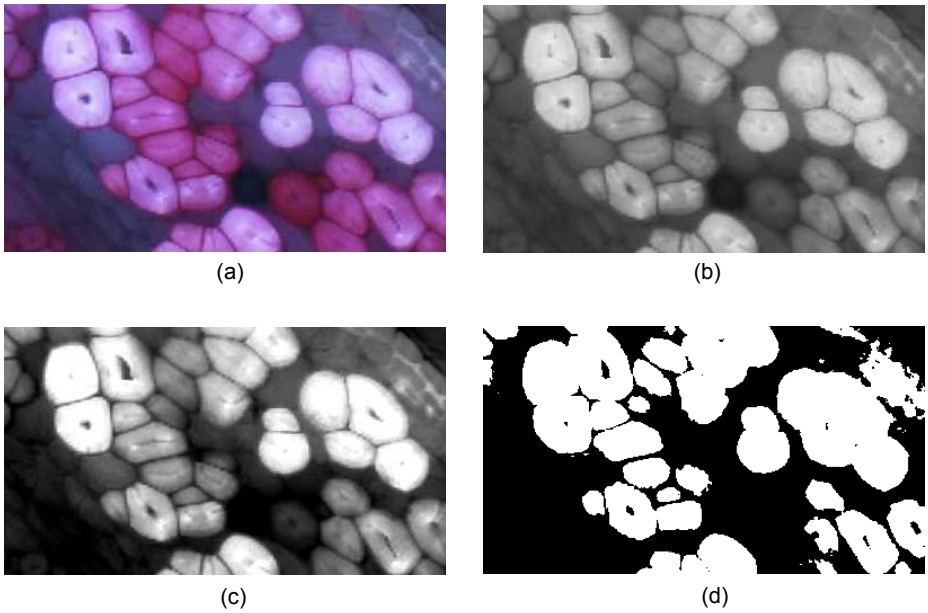


Fig. 2: a) Micrography, b) grayscale, c) constrast enhanced and d) Otsu's method threshold applied to initial micrography.

## 2.2 Modelling

The 3D model used for this study is based on a model previously developed in our team. It is fully described in [16] and [14]. It is based on macroscopic considerations and uses the continuum mechanics formulation. It uses the approach proposed by Marklund and Varna and by Neagu and Gamstedt, developed for multilayers orthotropic phase materials with helical structure and for an arbitrary number of phases and layers. The single fibre is modelled as a single-layered or multi-layered, thick-walled tube made of an orthotropic material having a helical orientation (corresponding to the cellulose microfibrils orientation). For this study only the $S_2$ is considered, since it is the main sub-layer of the cell wall in terms of thickness (almost 90%) and it contributes mainly to the global mechanical behaviour of the fibre. As explained in details in [14] and [16], during the simulation of the tensile test the fibre edges are kept free to rotate, to take into account local rotations that can occur in the cell wall.

### *2.2.1 Coordinate systems*

Regarding the coordinate systems used throughout this study, in addition to the global coordinate system related to the fibre $(\vec{X}, \vec{Y}, \vec{Z})$, a local coordinate system $(\vec{e}_\vartheta, \vec{e}_z, \vec{e}_r)$ was defined at each point of the fibre (Fig. 3). The working plane is defined as $(\vec{e}_\vartheta, \vec{e}_z)$, and the MFA in each layer is measured with respect to the fibre axis $(\vec{z} \equiv \vec{e}_z)$, and defined by $\beta_j$. A material coordinate system $(\vec{n}, \vec{t}, \vec{e}_z)$

is defined by a rotational angle of $\frac{\pi}{2} - \beta_j$, in order to express the isotropic transverse behaviour of the composite, in a material coordinate system related to the orientation of the microfibrils.

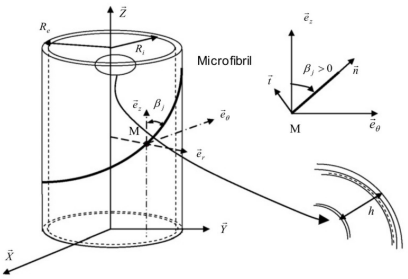


Fig. 3: Schematic representation of the elementary fibre with coordinate systems.

*2.2.2 Constitutive law*

Since the fibre wall is composed of polymeric constituents, for this study an anisotropic viscoelastic constitutive law is used.

The elastic properties of the fibre wall (longitudinal and transverse moduli $E_L$, $E_T$, Poisson's ratio $\nu_{LT}$ and shear modulus $G_{LT}$) were computed using a multi-scale rule of mixture technique and the properties of the main constituents of the cell wall [16]. The wall is considered as a long fibre-reinforced composite material in which the fibres are represented by the cellulose microfibrils and the matrix is considered as a mixture of transverse isotropic amorphous cellulose (hemicellulose) and isotropic lignin. The mechanical properties of the microfibrils are computed considering each microfibril as a cristallite of 6x6 unit cells in transverse section [14] covered with an outer surface of amorphous cellulose. So, the homogenisation technique for microfibrils is applied considering the properties and the volume fractions of crystalline and amorphous cellulose. In the same way, the elastic properties of the matrix are obtained using properties and volume fractions of the lignin and the hemicellulose. Finally, the properties of the cell wall are computed using the homogenised properties obtained for microfibrils and matrix.

Assuming that the local state of the material is completely defined by the elastic strain tensor $\underline{\varepsilon^e}$ and a set of second order tensors $\underline{\xi_i}(i \in \mathbb{N})$ corresponding to elementary mechanisms of viscoelastic flow, the state law leads to Eq. 7:

$$\dot{\underline{\varepsilon}} - \dot{\underline{\varepsilon^{ve}}}(\underline{\xi_i}; \underline{\varsigma}) = \underline{\underline{S^e}}\,\dot{\underline{\sigma}} \tag{1}$$

where $\dot{\underline{\sigma}}$ is the Cauchy true stress tensor, $\underline{\underline{S^e}}$ the elastic compliance tensor (2) corresponding to a transverse isotropic behaviour with respect to the microfibrils

direction, $\underline{\varepsilon^{\mathrm{ve}}}$ the viscoelastic strain tensor and $\varepsilon$ the total strain tensor such as $\underline{\varepsilon} = \underline{\varepsilon^{\mathrm{e}}} + \underline{\varepsilon^{\mathrm{ve}}}$.

$$\underline{\underline{S^{\mathrm{e}}}} = \begin{pmatrix} \frac{1}{E_L} & \frac{-\nu_{TL}}{E_T} & \frac{-\nu_{TL}}{E_T} & 0 & 0 & 0 \\ \frac{-\nu_{TL}}{E_T} & \frac{1}{E_L} & \frac{-\nu_{TL}}{E_T} & 0 & 0 & 0 \\ \frac{-\nu_{TL}}{E_T} & \frac{-\nu_{TL}}{E_T} & \frac{-\nu_{TL}}{E_T} & 0 & 0 & 0 \\ 0 & 0 & 0 & \frac{1}{G_{LT}} & 0 & 0 \\ 0 & 0 & 0 & 0 & \frac{1}{G_{LT}} & 0 \\ 0 & 0 & 0 & 0 & 0 & \frac{1}{G_{TT}} \end{pmatrix} \tag{2}$$

The viscoelastic model is based on the spectral-type one proposed by Boubakar et al. [41] and fully described in [16]. Following [41], the viscoelastic flow rule is given by:

$$\underline{\dot{\varepsilon^{\mathrm{ve}}}} = \sum_{i=1}^{n} \underline{\dot{\xi}_{\mathrm{i}}} = \sum_{i=1}^{n} \frac{1}{\tau_{\mathrm{i}}} \left( \mu_{\mathrm{i}} \underline{\underline{S^{\mathrm{ve}}}} \sigma - \underline{\xi_{\mathrm{i}}} \right) \tag{3}$$

where $\underline{\underline{S^{\mathrm{ve}}}}$ is a viscoelastic compliance tensor (4) whose general form is derived by considering an isotropic transverse behaviour with respect to the microfibrils direction, which is assumed to be purely elastic:

$$\underline{\underline{S^{\mathrm{ve}}}} = \begin{pmatrix} 0 & 0 & 0 & 0 & 0 & 0 \\ 0 & \frac{\beta_T}{E_T} & \frac{-\beta_{TT}\nu_{TT}}{E_T} & 0 & 0 & 0 \\ 0 & \frac{-\beta_{TT}\nu_{TT}}{E_T} & \frac{\beta_T}{E_T} & 0 & 0 & 0 \\ 0 & 0 & 0 & \frac{\beta_{LT}}{G_T} & 0 & 0 \\ 0 & 0 & 0 & 0 & \frac{\beta_{LT}}{G_T} & 0 \\ 0 & 0 & 0 & 0 & 0 & \frac{\beta^*}{G_{TT}} \end{pmatrix} \tag{4}$$

Where $\frac{\beta^*}{G_{TT}}$ is defined as:

$$\frac{\beta^*}{G_{TT}} = 2\left( \frac{\beta_T}{E_T} + \frac{\beta_{TT}\nu_{TT}}{E_T} \right) \tag{5}$$

Such a tensor requires, in addition to the classical elastic parameters, the identification of three parameters $(\beta_T, \beta_{TT}, \beta_{LT})$ related to the viscoelastic behaviour.

The viscoelastic parameters $(\beta_T, \beta_{TT}, \beta_{LT})$ were identified using inverse method from creep tests on single hemp fibres, combined with the use of the aforementioned spectral model and a hybrid minimisation algorithm [42],[43].

Regarding the spectral model, Eq. 5, for a given i value, $\mu_i$ and $\tau_i$ represent respectively the relative weight and the corresponding release time. A triangular spectral model is used in this work to define a distribution function of $\mu_i$ with respect to log $(\tau_i)$ under the following condition:

$$\sum_{i=1}^{n} \mu_i = 1 \tag{6}$$

This kind of spectrum is defined by its centre $\mathrm{zn_c}$ and its half-width $\mathrm{zn_0}$ as shown in Fig. 4 where $\Delta$ depends on both these quantities and on the number n of elementary mechanisms. For this study, thirty-one elementary mechanisms are used.

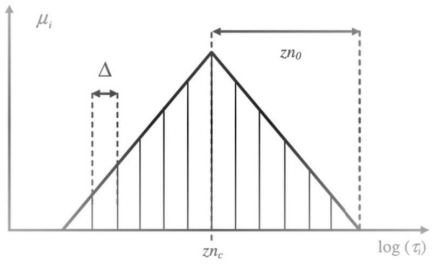


Fig. 4: Spectral model for the release times.

The values of the elastic properties and the viscoelastic parameters are summarised in Table 2.

| Elastic properties | | Viscoelastic parameters | |
|---|---|---|---|
| $E_L$ | 75 GPa | $\beta_{LT}$ | 12.25 |
| $E_T$ | 11 GPa | $\beta_T$ | 1.5 |
| $\nu_{LT}$ | 0.153 | $zn_c$ | 2.45 |
| $G_{LT}$ | 2.52 GPa | $zn_0$ | 1.9 |
| $\nu_{TT}$ | 0.2 | | |

Table 2: Elastic and viscoelastic parameters of the fibre wall material used in FE simulations.

The model is able to take into account both dislocations and the possible variations in cellulose microfibrils orientation along the fibre length [16]. The mechanical behaviour of the fibre is expressed through the material rotating frame formulation proposed in [14]. The coordinate systems used in this study (global and local) are also described in [14].

*2.2.3 FE model*

For cylindrical fibres with thin or thick wall, analytical solutions can be obtained [14]. For more complex geometries, FE computation is required. A toolbox dedicated to the modelling of the fibre has been created in Matlab® environment for this study. The coded scripts are able to automatically generate the fibre geometry and mesh and the setting data file for the finite element calculation performed in the FE Abaqus® code. Solid 8-nodes-element mesh is used for the finite elements analysis. The discretisation is performed using 40 elements in the section contour (both outer and inner perimeter), 80 elements in the length of the fibre and 5 elements in the wall thickness. Regarding the tensile test simulations, they are carried out applying the loading in two different ways. In the first way, a nodal displacement of both the edges of the fibre is applied. In the second one, a pressure loading is applied on the cross-section area at one extremity of the fibre, the other one being embedded. In both cases the amplitude of the load is chosen in order to

obtain an average strain rate equal to the usual experimental one, which is approximately $5 \cdot 10^{-4}$ $s^{-1}$. The maximum global strain level reached during the simulation is 4%. This relatively high value is neverthless consistent with the distributions of properties reported in the literature. According to Duval et al.[11] and Keller [21] for example, deformation at failure for hemp fibres may reach greater values than to the above mentioned 4%. So, the value of maximum deformation equal to 4% is chosen in order to consider a larger amount of fibres.

Since the experimental results are always expressed in term of global tensile behaviour, for the simulation both global axial strain and stress have to be computed in the same way as the experimental protocol for the tensile test on elementary fibres requires. The global axial strain is obtained as the ratio between the applied displacement and the initial length of the fibre. Regarding the global stress, when the nodal displacement is applied, it is computed in two steps : firstly by summing all the reactions at the imposed displacement, in order to obtain a global reaction force. This force is then divided by the initial cross-section area of the sample, in order to obtain the global stress. In the case of the pressure load, the global stress corresponds directly to the applied load. In both cases, the variations of the surface of the cross-section during the simulation is negligible (less than 1%). The results shown later, unless otherwise specified, are carried out applying the nodal displacement at the edges of the fibre.

Once the global stress-strain curve obtained, the apparent tangent Young's modulus is expressed as a function of the global strain. Simulations are carried out using a quad-core dual processor system, with 36GB of RAM.

#### *2.2.4 Modelling the fibre morphology*

Once the contour lines obtained from optical image processing, a discretization of the outer and inner perimeters was performed, in order to create a 2D mesh for the cross-section in the $(x,y)$ plane. The 3D geometry is then obtained by extrusion of the 2D mesh in the $z$ direction and the section is kept constant along the length of the fibre. During this study some simulations were also carried out accounting for the variations of cross-section along the fibre length. The modelled geometries in this case were inspired by the results proposed in [44] for hemp fibres and in [45] and [46] for flax fibres. The variations of the cross-section were taken into account using a sinusoidal variation of the diameter dimension along the fibre length. The diameter variations were kept between 10% and 25%, which is consistent with the data proposed in the literature [44; 45]. Fig. 5 shows a model of a fibre with a maximum variation of the cross-section surface ($\Delta S_{\max}$) equal to $\pm$20%.

The real morphology reconstruction method is expensive in terms of computation time, and it's not suitable to perform repetitive analysis such as, for example, sensitivity analysis. A less expensive method to model the 3D morphology of the fibre is to automatically generate simplified shapes of the cross-section, neglecting the irregularities of the real contour lines. The method implemented in Matlab® environment generates 3D geometry and mesh using just a few parameters as input, such as the largest diameter, the length of the sample, the cross-section area and the so-called degree of ellipticity of the section, defined as:

$$e = 1 - \frac{b}{a} \tag{7}$$

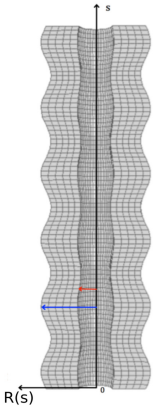


Fig. 5: Model with sinusoidal variation of the diameter along the fibre length.

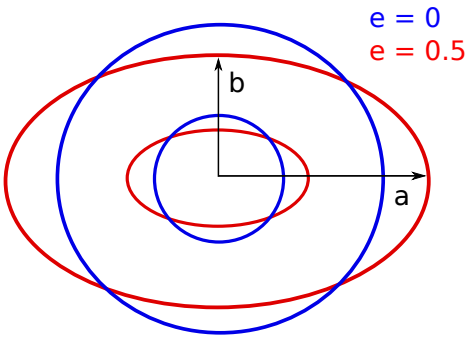


Fig. 6: Modelled simplified cross-sections.

Where a and b are respectively the largest and the smaller outer diameter of an ellipse, as shown in Fig. 6. As for the generation of the real morphology model, a first 2D mesh of the section is created and then extruded in the z direction to obtain the 3D model.

Regarding the dimensions of the lumen, an homothetic transformation is applied, so the $e$ parameter for the outer and the inner perimeter is the same for each geometry. In order to quantify the difference between a real cross-section and a perfectly elliptical one, the classical least square formulation were used to compute the amplitude of irregularities:

$$\alpha = \frac{\sqrt{\sum_{k=1}^{N} \frac{(R_r - R_s)^2}{R_r^2}}}{N} \tag{8}$$

Where $R_r$ and $R_s$ are the radius in each discretisation point of, respectively, the real and the simplified (elliptical) contours. N is the total number of discretisation points of the perimeter.

## 3 Results and discussions

### 3.1 Fibres morphology characterisation

Results of the fibre morphology characterisation are shown in Table. 3.

| | Largest diameter [$\mu m$] | Smallest diameter [$\mu m$] | Fibre wall surface [$\mu m]^2$] | Lumen surface [$\mu m]^2$] | e [-] |
|---|---|---|---|---|---|
| Mean | 49.1 | 32.6 | 1260.8 | 83.9 | 0.3 |
| Max | 72.6 | 50.5 | 1983.4 | 231.1 | 0.7 |
| Min | 31.5 | 14.1 | 325.0 | 0 | 0.01 |

Table 3: Measured geometric parameters on real fibre morphologies.

These data were collected on 30 fibres, starting from the Fig. 1. This amount of fibres is insufficient to ensure a statistically reliable characterisation, of which, by the way, literature is rich [11; 33–35; 44]. However, the experimental observation is necessary since, to the best of our knowledge, there are no data available in the literature regarding the contour lines definition of hemp fibres. Results in terms of mean diameter and fibre wall surface are consistent with those proposed in literature [35], [44]. The mean value of the degree of ellipticity $e$ is also consistent with the value suggested by Gassan et al. [40] as a realistic maximum value for the degree of ellipticity of plant fibres. Fig. 7 shows three reconstructed morphologies obtained using the pattern recognition tool: for each fibre, the approximated elliptical shape and the amplitude of irregularities are computed using the least square formulation described above. The degrees of ellipticity are obtained from the approximated elliptical morphologies. For the analysed fibres, the irregularities lie between $\alpha = 0.02$ and $\alpha = 0.17$.

### 3.2 Numerical simulation of the tensile behaviour: real vs simplified morphology

A comparaison between the tensile behaviour obtained for the real shaped fibres and the approximated ones is performed. The numerical simulations, unless otherwise specified, are carried out using the viscoelastic constitutive law, in which the material parameters are the same defined in Table 2 and the reorientation of the microfibrils is taken into account (starting from MFA=11°). For these fibre shapes and amplitude of irregularities ($\alpha$), results of numerical simulation (Fig. 8) show that the irregularities of the morphology do not highly affect the global tensile behaviour of the fibre. In this case, the cross-section is kept constant along the fibre length.

The shape of the tensile response (Fig. 8) is almost the same in both real and simplified modelled morphologies. Neverthless, starting from the 3% of strain, the apparent tangent modulus trend of the real-shaped *Fibre 3* begins to slightly diverge from the simplified elliptical one. *Fibre 3* is the fibre modelled with the greatest value of irregularities ($\alpha = 0.17$, Fig. 7). This discrepancy suggests that a larger amplitude of irregularities may involve an effect on the apparent stiffness

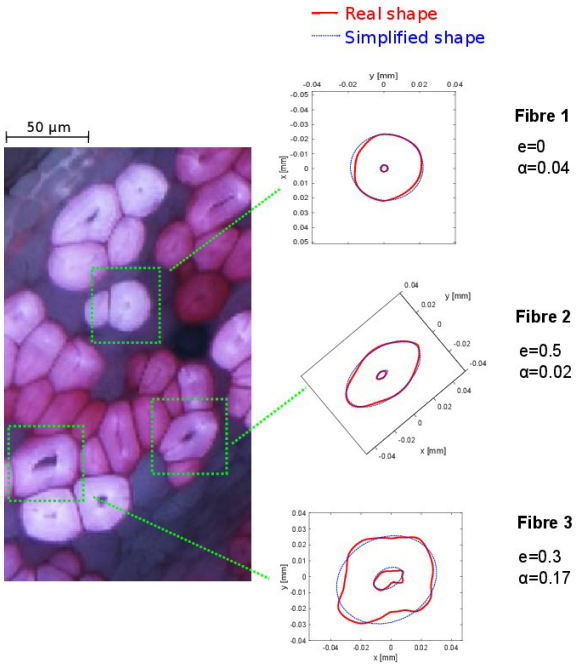


Fig. 7: Morphology reconstruction of three primary hemp bast fibres.

of the elliptic fibre. Moreover an irregular perimeter of the cross-section do have an influence on the evolution of stress concentration, as shown in Fig. 9, and so, probably, on the rupture behaviour.

Irregularities in the cross-section contour clearly induce stress heterogeneity in the fibre wall. This will necessarily modify the damage propagation in the fibre wall and the failure behaviour of the fibre. Similar results are obtained applying a variation of the cross-section along the fibre length, using, for example, the geometry shown in Fig. 5, which represents the most unfavourable case. Fig. 10 shows the tensile responses obtained for four modelled geometries: perfectly circular cross-section shape ($e$=0), constant (I) or varying (II) along the length of the fibre, and elliptical cross-section shape ($e$=0.5), constant (III) or varying (IV) along the length of the fibre. Maximum variation of cross-section surface for cases (II) and (IV) is set to ±20%.

Here again the variation of the cross-section along the length of the fibres does not affect the shape of the tensile behaviour. The observed gap between cases (I) and (II) and between (III) and (IV) is a consequence of a decrease of the global stiffness beacause of the local decrease in the cross-section. It induces strong stress concentrations, as shown in Fig. 11, and this may influence the failure behaviour of the fibre.

The analysis of the rupture phenomena is beyond the scope of this study, so we propose, in a first approach, to investigate the influence of non-zero degrees of ellipticity of simplified (elliptical) morphologies on the global tensile behaviour of

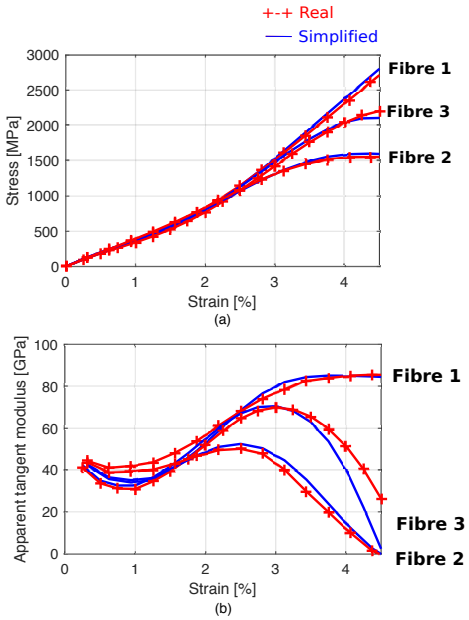


Fig. 8: Tensile behaviour (a) and apparent tangent modulus as a function of longitudinal strain (b) for complex and simplified cross-section shapes.

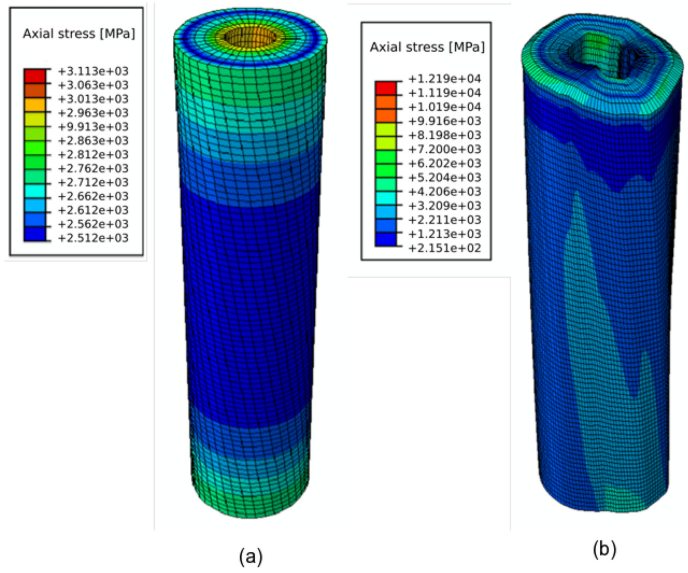


Fig. 9: Stress field for simplified (a) and irregular (b) cross-section, with $e$=0.

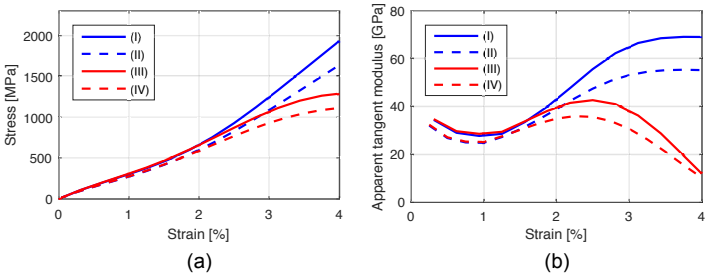


Fig. 10: Tensile behaviour (a) and apparent tangent modulus (b) for fibre with cross-section surface constant or varying along the length.

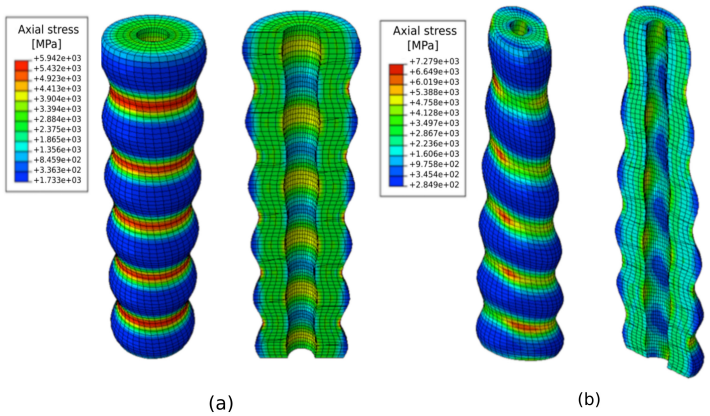


Fig. 11: Stress field for cylindrical (a) and elliptical (b) fibres with cross-section variations along the length ($\Delta S_{\max} = \pm 20\%$).

the elementary fibre, neglecting the cross-section variations along the fibre length. The aim is, in particular, to investigate the influence of the degree of ellipticity of the fibre section on the non-linear behaviour of the sample.

### 3.3 Numerical simulation of the tensile behaviour: Influence of the degree of ellipticity

In order to evaluate the influence of the degree of ellipticity of the cross-section of the fibre on its tensile response, results obtained for elliptic geometries are compared. The elliptical cross-sections are modelled with $e$ varying from 0 to 0.7. This interval span is chosen to match the experimental data. For each modelled geometry, the cross-section area is kept constant along the length of the fibre. To avoid any effect due to the variation in the cross-section surface, the surface is kept constant for each tested fibre, as shown in Table 4. The idea is to focus this study only on the effect of the $e$ parameter. The dimensions of the diameters and, by

| e | a [$\mu m$] | b [$\mu m$] | a' [$\mu m$] | b' [$\mu m$] |
|---|---|---|---|---|
| 0 | 13.3 | 13.3 | 4.46 | 4.46 |
| 0.3 | 18.2 | 10.8 | 5.47 | 3.3 |
| 0.5 | 18.8 | 9.4 | 6.2 | 3.1 |
| 0.7 | 24.3 | 7.3 | 8 | 2.4 |

Table 4: Values of cross-section features for different values of $e$ and for a constant wall area of 493 $\mu m^2$ .

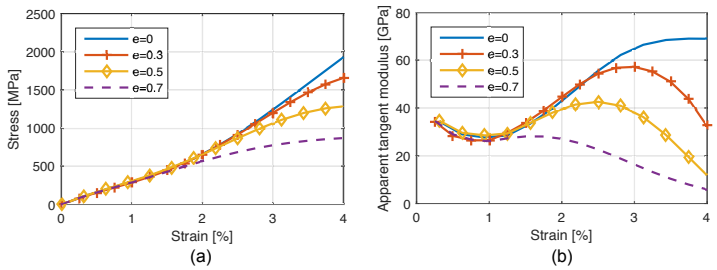


Fig. 12: Stress-strain curves (a) and apparent tangent modulus (b) computed for models with diffent values of $e$.

consequence, of the surface area, are neverthless chosen in the range of amplitude reported in literature (Table 1).

The simulations are carried out using the parameters values synthesised in Table 2. As shown in Fig. 12a and 12b, the tensile behaviour is greatly influenced by the shape of the section and in particular by the parameter $e$. When fibres are modelled as perfect cylinders, results show a behaviour with three phases: (1) a quasi-linear response for small deformations, followed by (2) a decrease in the stiffness then (3) a slightly parabolic reflecting an increase in the stiffness. For elliptical cross-sections, curve bends especially as the axial strains are large. This shift is even more significant for higher value of $e$. Non-zero values for the degree of ellipticity of the cross-section involve in particular a strong decrease of the apparent stiffness, starting at lower value of axial strain for higher value of the degree of ellipticity. This kind of behaviour is similar to the second type of response experimentally observed by Placet et al. [27]. Authors showed that hemp fibres express three particular kinds of quai-static behaviour: the second one, with a strong decrease of the apparent stiffness seems to be close to the one computed for fibres modelled as elliptical tubes.

According to Gassan [40] a realistic value for the $e$ parameter should not be higher than 0.4. Although, even for elliptical fibre with $e = 0.3$ simulation results show a loss of apparent stiffness around 15% compared to the cylindrical one at 3% of axial strain and a decrease of almost 50% in stiffness at the maximum strain level (Fig. 12b). The obtained results suggest that it might exist a relationship between the non-linear behaviour experimentally observed for hemp fibres and their morphological characteristics, such as the value of the $e$ parameter, for example.

### 3.4 Investigating the origins of the geometric effect

In order to accurately identify and understand the relationship between the tensile behaviour and the morphology of the fibre, numerical simulations of the tensile tests were also performed using different constitutive laws for behaviour of the the fibre wall. Effectively, the non-linear behaviour results from a coupling or a combination between morphologic parameters and other physical mechanisms, such as ultrastructural parameters (MFA) and parameters of the constitutive behaviour law (viscoelastic parameters, in particular).

#### *3.4.1 Influence of the elastic anisotropy of the fibre wall material*

In Table 5 are summarised the material parameters used to investigate the influence of the anisotropy of the fibre wall material on the tensile response.

| | Type | Elastic parameters | MFA | Cellulose MF reorientation |
|---|---|---|---|---|
| SIM 1 | Isotropic | $E = 40$ GPa<br>$\nu = 0.2$ | 11° | No |
| SIM 2 | Anisotropic | $E_L = 75$ GPa<br>$E_T = 11$ GPa<br>$\nu_{LT} = 0.153$<br>$G_{LT} = 2.52$ GPa<br>$\nu_{TT} = 0.2$ | 11° | No |
| SIM 3 | Anisotropic | $E_L = 75$ GPa<br>$E_T = 11$ GPa<br>$\nu_{LT} = 0.153$<br>$G_{LT} = 2.52$ GPa<br>$\nu_{TT} = 0.2$ | 11° | Yes |

Table 5: Material elastic parameters used for the simulations.

The first kind of elastic law is an isotropic one (SIM 1): in this case, the elastic properties used to feed the model are obtained using the rule of mixture technique considering the microfibrils parallel to the fibre axis. The computed global behaviour and apparent tangent modulus shapes are shown in Fig. 13a and 13b. In this case, the stress-strain curves and the apparent stiffness-strain curves are perfectly superimposed for each value of the $e$ parameter of the cross-section. That means that the non-linearity observed in Fig. 12 is not related to a purely geometrical effect. Results shown in Fig. 13c and 13d are obtained using an elastic constitutive law and considering the fibre wall as an anisotropic material (SIM 2) : in this case a microfibrils angle (MFA) of 11° is considered and the reorientation of cellulose microfibrils under tensile loading is not taken into account. The global behaviour shown in Fig. 13c doesn't show a remarkable effect of the $e$ parameter, but the apparent stiffness curves in Fig. 13d exhibit a small decrease of the apparent tangent modulus for the fibre with the highest value of $e$ (decrease of around 10% compared to the perfectly cylindrical fibre stiffness at 4% of global strain).

When taking into account the possible reorientation of cellulose microfibrils under tensile loading (SIM 3), an additional loss in stiffness is observed (Fig 13d

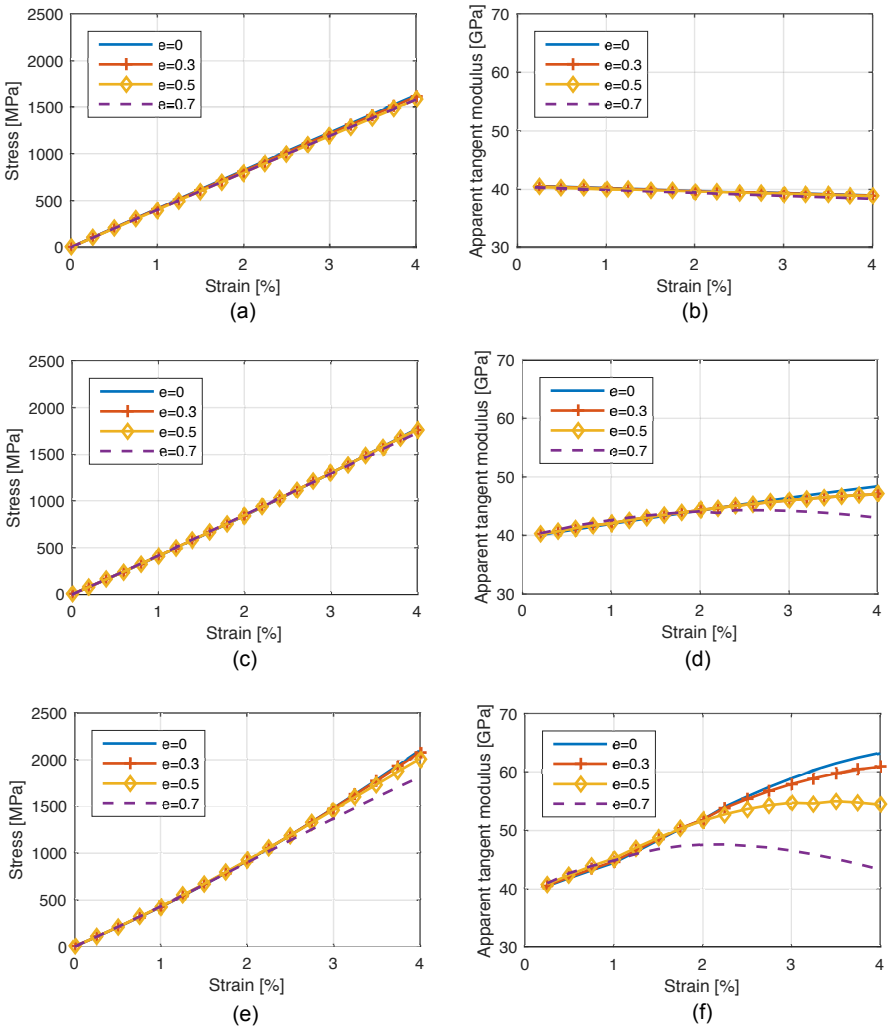


Fig. 13: Stress-strain curves obtained using different elastic constitutive law: SIM 1 (a-b), SIM 2 (c-d) and SIM 3 (e-f).

and 13f), even for lower values of the degree of ellipticity. The decrease of the apparent stiffness is also observed on the global tensile behaviour in Fig. 13e. These simulations, performed considering an elastic behaviour of the fibre wall material, suggest that the geometrical effect is expressed only when this material is anisotropic and sharpened when the reorientation of cellulose microfibrils is taken into account.

*3.4.2 The influence of the MFA*

Since the geometrical effect seems to be strongly related to the ultrastructure of the fibre wall, it is interesting to evaluate the influence of the initial micro-fibrillar angle (MFA) on the shape of the tensile response. Simulations have been carried out using an elliptical cross-section fibre with different values of initial MFA.

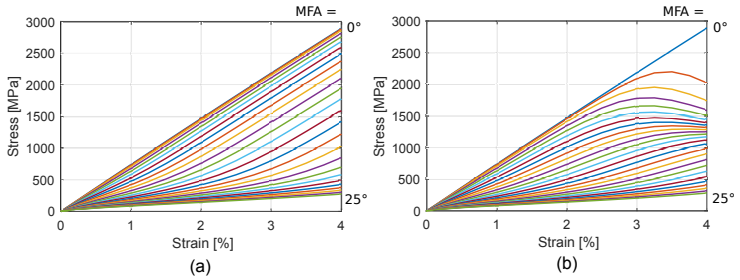


Fig. 14: Stress-strain curves for a cylindrical (a) and elliptical (b) fibre, computed with different values of the initial MFA.

As shown in Fig. 14a and 14b, for some MFA considered, in particular for MFA=0° and MFA≥ 17°, the global behaviour obtained for an elliptic section ($e = 0.5$) or cylindrical one overlap. But for cellulose microfibrils angles between 1° and 16°, it is possible to observe a change of the shape of the stress-strain curve and a stiffness decrease when the fibre has an elliptical cross-section in comparison to the cylindrical shaped one. This result confirms that the geometrical effect is dependent on the anisotropy ratio of the transversely isotropic material constituting the fibre wall. This phenomenon is activated and enhanced by the time-dependency of the material. Indeed, Fig. 15 shows the comparison between the tensile behaviours obtained using elastic (cf. Table 5, SIM 3) and viscoelastic (Cf. Table 2) constitutive laws. In both cases, the microfibrils reorientation is taken into account (initial MFA is 11°) and cylindrical and elliptical ($e$=0.5) shapes are used.

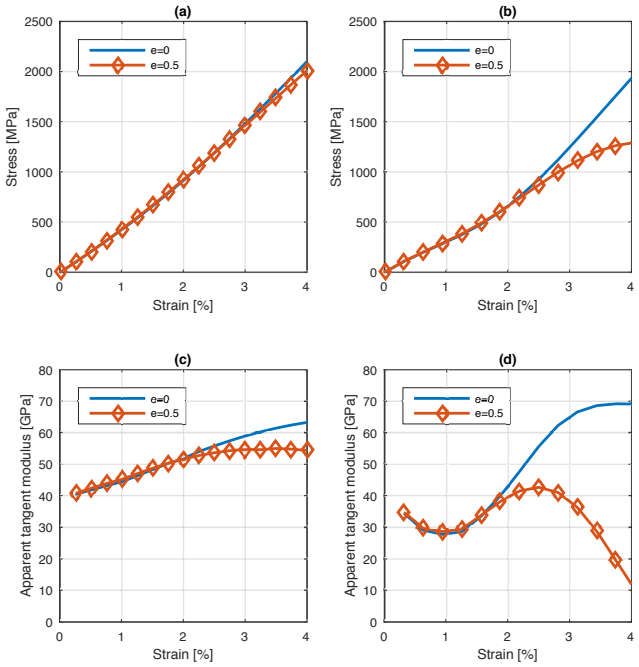


Fig. 15: Tensile behaviour of cylindrical and elliptical fibres using two anisotropic constitutive laws: elastic (a-c) and viscoeleastic (b-d).

At the maximum strain level, when the time-dependency of the fibre wall material is neglected, the loss of apparent stiffness occurring in the case of elliptical fibre is about 22% when compared to the cylindrical one (Fig. 15 c). The decrease in stiffness for the elliptical fibre reaches a value of 85% when, on the contrary, the viscoelasticity is taken into account (Fig. 15 d). So, the tensile responses plotted in Fig. 15 show that the geometrical effect is highly influenced by the viscoelasticity of the fibre wall material.

### 3.5 Towards an explanation of the geometric effect

In order to give a proper interpretation of the obtained results, the evolution of the local stress-strain fields in the elliptical fibre cross-section, with $e$=0.5, is shown in Fig. 16 and in Video 1. The chosen section is placed far from the edges of the fibre, at almost a quarter of the global length of the sample. The shear stress and strain are respectively $\tau_{\vartheta z}$ and $\varepsilon_{\vartheta z}$ in the classical cylindrical coordinate system. Both axial and shear fields show strong stress concentration zones, especially on the outer perimeter of the fibre. As shown in Fig. 16, the stress fields in the section of the elliptic fibre is strongly heterogeneous in the wall thickness. In particular,

both shear stress and strain show negative to positive transition zones during the tensile test simulation, in both inner and outer perimeters (Fig. 17 and Video 2).

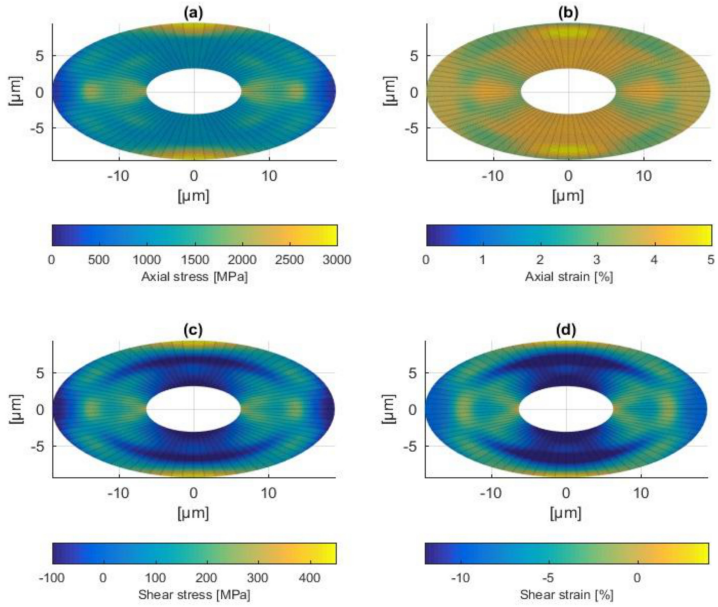


Fig. 16: Local fields in the elliptical cross-section at 4% of global strain: axial stress (a) and strain (b), shear stress (c) and strain (d).

This kind of mechanical behaviour has already been observed for thin-walled anisotropic cylinders [47; 48] and wood fibres [49] in which the non-linearity of the stress-strain curve is attributed to the evolution of wall buckling phenomena when the fibre is tensile loaded. In the case of wood fibres, Page [26] observed that the apparition of wall buckling under tension involves a loss of axial stress, which leads consequently to a decrease in the apparent stiffness.

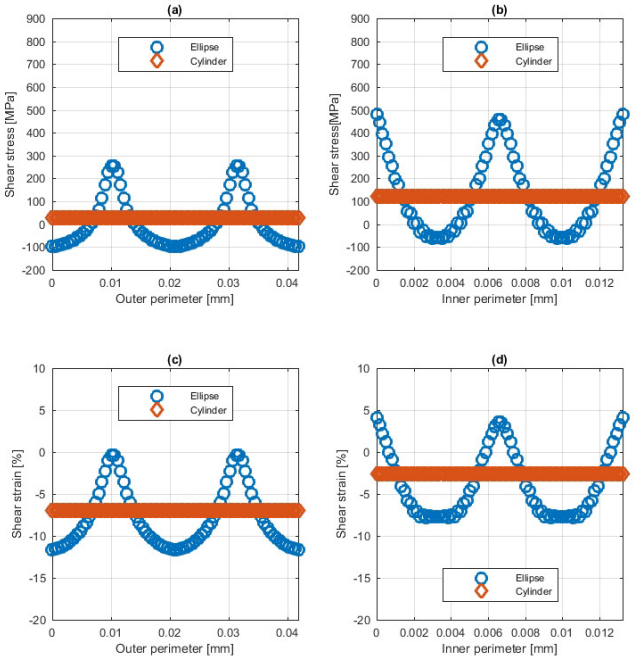


Fig. 17: Local fields along the outer and inner perimeters for cylindrical and elliptical morphologies at 4% of global strain: shear stress (a-b) and strain (c-d).

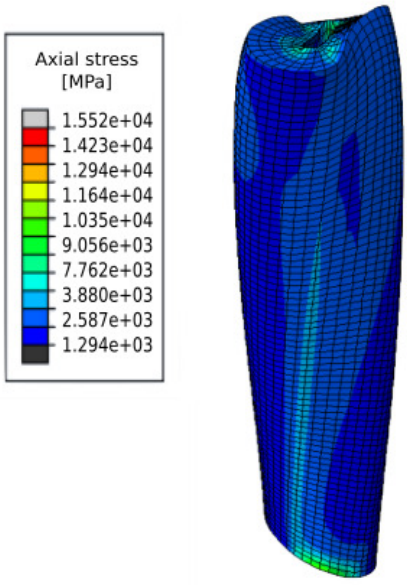


Fig. 18: Elliptical fibre during a tensile test simulation with applied pressure.

However, Page suggested that in the case of thick wall the fibres resist to tension buckling. Results of our simulations suggest that even if the buckling under tension is nonexistent because of the thickness of the fibre wall, the strongly heterogeneous shear stress and strain fields lead to a global loss of the apparent stiffness of the fibre. Fig. 18 shows a fibre during a tensile test simulation when pressure is applied. The value of MFA is equal to 11° and the reorientation of the microfibrils is taken into account. The viscoelasticity of the fibre wall material is also taken into account. Fig. 18 shows that the upper edge of the fibre, on which the pressure is applied, exhibits a very complex shape, typical of the anisotropic materials. The axial displacement of the upper surface is strongly heterogeneous, with some regions that seem to be easier to deform and, on the contrary, others that seem to collapse. This results suggest that, when the nodal displacement is applied, the apparition of shear stress concentrations involves a loss of apparent stiffness because they contribute to the axial deformation of the fibre wall. This interpretation is confirmed by the results showing the local fields of shear stress and strain for elliptical fibres with different values of MFA. As shown above (Fig. 12), for MFA values between 1° and 16° the global tensile behaviour shows a change in the shape of the non-linearity, with a significant decrease of the apparent stiffness from a yield point corresponding to an axial strain value of approximately 2%. In order to relate the computed global behaviour to the local one, Fig. 19 shows the local stress and strain field for three fibres with different values of MFA, one inside the range $1° \leq MFA \leq 17°$ and the others ones outside it. Observing the local stress and strain fields evolution for elliptical fibres ($e$=0.5) with a MFA equal to 11°, 0° and 25° (Fig. 19 and Video 3), results show that the shear stress and strain fields have strongly different shapes along the contour lines. In the case of an MFA equal to 11°, shear stresses and strains exhibit a strong variation, significantly increasing especially when approaching to the smallest diameter value of the elliptic shape. On the contrary, in the case of MFA equal to 0° and 25° this variation is far less pronounced. This result is consistent with the interpretation described above, in which the non-linearity of the behaviour observed for elliptical fibres, involving a decrease of the apparent stiffness starting from a yeld point, is strongly related to the local shear behaviour in the thickness of the fibre wall itself. Fig. 18 and Fig. 19 also show very high values of stress for both axial (Fig. 18 b) and shear stresses (Fig. 19 b). These extreme values are clearly not realistic and are for sure not observable since they overpass the strength of the material of the fibre wall. So, it seems important in future work to take into account the damage and failure phenomena by introducing failure criterion and damage mechanisms in the behaviour law.

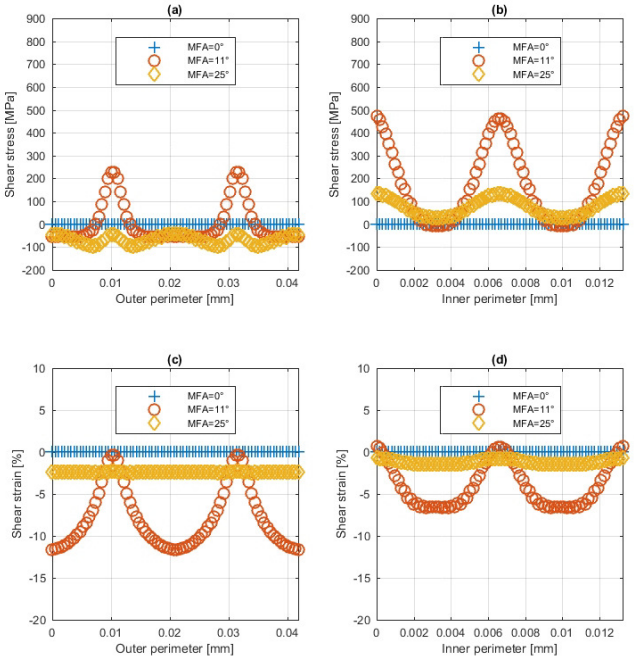


Fig. 19: Local fields along the outer and inner perimeters for elliptical morphologies with different values of MFA at 4% of global strain: shear stress (a-b) and strain (c-d).

## 4 Conclusions

Results presented in this paper and obtained using numerical simulations, show that the non-linear tensile behaviour of primary hemp fibres is affected by the morphology. Real and elliptical cross-section shapes were modelled and the obtained results show that the degree of ellipticity has a dominant influence on the tensile behaviour of the fibre. This geometrical effect is dependent on the anisotropy ratio of the transversely isotropic material constituting the fibre wall and enhanced by the viscoelasticity.

The anisotropy of the material is driven by the MFA. This study particularly points out the remarkable influence of MFA on the non-linearity of the tensile behaviour of the fibre, especially when an elliptical geometry is considered The non-linearity of the stress-strain curve is, in particular, characterised by a decrease in the apparent stiffness of the fibre from a yield point of approximately 2% in axial strain..

A possible interpretation of this relationship between morphology/anisotropy and global tensile behaviour of hemp fibres is the generation of highly heterogeneous local fields of stress and strain (both axial and shear) in the elliptical cross-section.

The work initiated in this paper will continue in the near future covering the modelling of the damage mechanisms occurring into the fibre wall and the analysis of the rupture phenomena. It is also the starting point of a more extended work intended to the characterisation of the propagation of the non-linear tensile behaviour from the isolated hemp fibre to the larger scales of continuous renforcements and composite plies.

## 5 Aknowledgments

The authors would like to aknowledge Camille François, PhD student at the Department of Applied Mechanics of the FEMTO-ST Institute for preparing the hemp samples and providing the images used for the microscopic observations.

## References

1. J. Summerscales, N. Dissanayake, A. Virk, W. Hall, A review of bast fibres and their composites. Part 2 Composites, Compos. Part A Appl. Sci. Manuf. 41 (2010) 1336–1344.
2. A. Bledzki, Composites reinforced with cellulose based fibres, Prog. Polym. Sci. 24 (2) (1999) 221–274.
3. O. Faruk, A. K. Bledzki, H.-P. Fink, M. Sain, Biocomposites reinforced with natural fibers: 20002010, Prog. Polym. Sci. 37 (11) (2012) 1552–1596.
4. D. U. Shah, P. J. Schubel, M. J. Clifford, P. Licence, The tensile behavior of off-axis loaded plant fiber composites: An insight on the nonlinear stress-strain response, Polym. Compos. 33 (9) (2012) 1494–1504.
5. G. Lebrun, A. Couture, L. Laperrière, Tensile and impregnation behavior of unidirectional hemp/paper/epoxy and flax/paper/epoxy composites, Compos. Struct. 103 (2013) 151–160.
6. D. Scida, M. Assarar, C. Poilâne, R. Ayad, Influence of hygrothermal ageing on the damage mechanisms of flax-fibre reinforced epoxy composite, Compos. Part B Eng. 48 (2013) 51–58.
7. C. Poilâne, Z. E. Cherif, F. Richard, A. Vivet, B. Ben Doudou, J. Chen, Polymer reinforced by flax fibres as a viscoelastoplastic material, Compos. Struct. 112 (2014) 100–112.
8. F. d. A. Silva, N. Chawla, R. D. d. T. Filho, Tensile behavior of high performance natural (sisal) fibers, Compos. Sci. Technol. 68 (15-16) (2008) 3438–3443.
9. Bodros E, Baley C (2008) Study of the tensile properties of stinging nettle fibres (Urtica dioica). Mater Lett 62(14):2147–2149.
10. Sedighi Gilani, Marjan, A micromechanical approach to the behaviour of single wood fibers and wood fracture at cellular level, PhD thesis.
11. A. Duval, A. Bourmaud, L. Augier, C. Baley, Influence of the sampling area of the stem on the mechanical properties of hemp fibers, Mater. Lett. 65 (4) (2011) 797–800.
12. V. Placet, O. Cisse, M. L. Boubakar, Influence of environmental relative humidity on the tensile and rotational behaviour of hemp fibres, J. Mater. Sci. 47 (7) (2012) 3435–3446.

13. T. Nilsson, P. J. Gustafsson, Influence of dislocations and plasticity on the tensile behaviour of flax and hemp fibres, Compos. Part A Appl. Sci. Manuf. 38 (7) (2007) 1722–1728.
14. V. Placet, F. Trivaudey, O. Cisse, V. Gucheret-Retel, M. L. Boubakar, Diameter dependence of the apparent tensile modulus of hemp fibres: A morphological, structural or ultrastructural effect?, Compos. Part A Appl. Sci. Manuf. 43 (2) (2012) 275–287.
15. Virk AS, Hall W, Summerscales J (2012) Modulus and strength prediction for natural fibre composites. Mater Sci Technol 28(7):864–871.
16. F. Trivaudey, V. Placet, V. Guicheret-Retel, M. L. Boubakar, Nonlinear tensile behaviour of elementary hemp fibres. Part II: Modelling using an anisotropic viscoelastic constitutive law in a material rotating frame, Compos. Part A Appl. Sci. Manuf. 68 (2015) 346–355.
17. C. M. Altaner, M. C. Jarvis, Modelling polymer interactions of the molecular Velcro' type in wood under mechanical stress, J. Theor. Biol. 253 (3) (2008) 434–445.
18. J. Keckes, I. Burgert, K. Frühmann, M. Müller, K. Kölln, M. Hamilton, M. Burghammer, S. V. Roth, S. Stanzl-Tschegg, P. Fratzl, Cell-wall recovery after irreversible deformation of wood, Nat. Mater. 2 (12) (2003) 810–813.
19. N. Mostefai, R. Hamzaoui, S. Guessasma, A. Aw, H. Nouri, Microstructure and mechanical performance of modified hemp fibre and shiv mortars: Discovering the optimal formulation, Mater. Des. 84 (2015) 359–371.
20. E. Marklund, J. Varna, Modeling the Effect of Helical Fiber Structure on Wood Fiber Composite Elastic Properties, Appl. Compos. Mater. 16 (4) (2009) 245–262.
21. Keller A (2003) Compounding and mechanical properties of biodegradable hemp fibre composites. Compos Sci Technol 63(9):1307–1316.
22. R. J. Astley, K. A. Stol, J. J. Harrington, Modelling the elastic properties of softwood: Part II: The cellular microstructure, Holz als Roh- und Werkst. 56 (1) (1998) 43–50.
23. J. J. Harrington, R. J. Astley, R. Booker, Modelling the elastic properties of softwood: Part I: The cell-wall lamellae, Holz als Roh- und Werkst. 56 (1) (1998) 37–41.
24. I. Burgert, K. Frühmann, J. Keckes, P. Fratzl, S. Stanzl-Tschegg, Properties of chemically and mechanically isolated fibres of spruce (Picea abies[L.] Karst.). Part 2: Twisting phenomena, Holzforschung 59 (2).
25. A. Bourmaud, C. Morvan, A. Bouali, V. Placet, P. Perré, C. Baley, Relationships between micro-fibrillar angle, mechanical properties and biochemical composition of flax fibers, Ind. Crops Prod. 44 (2013) 343–351.
26. D. H. Page, F. El-Hosseiny, K. Winkler, Behaviour of Single Wood Fibres under Axial Tensile Strain, Nature 229 (5282) (1971) 252–253.
27. V. Placet, O. Cisse, M. Lamine Boubakar, Nonlinear tensile behaviour of elementary hemp fibres. Part I: Investigation of the possible origins using repeated progressive loading with in situ microscopic observations, Compos. Part A Appl. Sci. Manuf. 56 (2014) 319–327.
28. Thomason JL, Carruthers J, Kelly J, Johnson G (2011) Fibre cross-section determination and variability in sisal and flax and its effects on fibre performance characterisation. Compos Sci Technol 71(7):1008–1015.

29. K. Charlet, J.-P. Jernot, J. Breard, M. Gomina, Scattering of morphological and mechanical properties of flax fibres, Ind. Crops Prod. 32 (3) (2010) 220–224.
30. A. W. Blake, S. E. Marcus, J. E. Copeland, R. S. Blackburn, J. P. Knox, In situ analysis of cell wall polymers associated with phloem fibre cells in stems of hemp, Cannabis sativa L., Planta 228 (1) (2008) 1–13.
31. V. Placet, J. Méteau, L. Froehly, R. Salut, M. L. Boubakar, Investigation of the internal structure of hemp fibres using optical coherence tomography and Focused Ion Beam transverse cutting, J. Mater. Sci. 49 (24) (2014) 8317–8327.
32. C. Mattrand, A. Béakou, K. Charlet, Numerical modeling of the flax fiber morphology variability, Compos. Part A Appl. Sci. Manuf. 63 (2014) 10–20.
33. T. Schäfer, B. Honermeier, Effect of sowing date and plant density on the cell morphology of hemp (Cannabis sativa L.), Ind. Crops Prod. 23 (1) (2006) 88–98.
34. D. Crônier, B. Monties, B. Chabbert, Structure and Chemical Composition of Bast Fibers Isolated from Developing Hemp Stem, J. Agric. Food Chem. 53 (21) (2005) 8279–8289.
35. H. S. Sankari, Comparison of bast fibre yield and mechanical fibre properties of hemp (Cannabis sativa L.) cultivars, Ind. Crops Prod. 11 (1) (2000) 73–84.
36. N. E. Zafeiropoulos, C. A. Baillie, A study of the effect of surface treatments on the tensile strength of flax fibres: Part II. Application of Weibull statistics, Compos. Part A Appl. Sci. Manuf. 38 (2) (2007) 629–638.
37. C. Baley, Analysis of the flax fibres tensile behaviour and analysis of the tensile stiffness increase, Compos. Part A Appl. Sci. Manuf. 33 (7) (2002) 939–948.
38. T. Joffre, A. Miettinen, F. Berthold, E. K. Gamstedt, X-ray micro-computed tomography investigation of fibre length degradation during the processing steps of short-fibre composites, Compos. Sci. Technol. 105 (2014) 127–133.
39. R. Ntenga, A. Beakou, Structure, morphology and mechanical properties of Rhectophyllum camerunense (RC) plant-fiber. Part I: Statistical description and image-based reconstruction of the cross-section, Comput. Mater. Sci. 50 (4) (2011) 1442–1449.
40. J. Gassan, A. Chate, A. K. Bledzki, Calculation of elastic properties of natural fibers, J. Mater. Sci. 36 (15) (2001) 3715–3720.
41. M. L. Boubakar, L. Vang, F. Trivaudey, D. Perreux, A mesomacro finite element modelling of laminate structures, Compos. Struct. 60 (3) (2003) 275–305.
42. V. Guicheret-Retel, O. Cisse, V. Placet, J. Beaugrand, M. Pernes, M. L. Boubakar, Creep behaviour of single hemp fibres. Part II: Influence of loading level, moisture content and moisture variation, J. Mater. Sci. 50 (5) (2015) 2061–2072.
43. O. Cisse, V. Placet, V. Guicheret-Retel, F. Trivaudey, M. L. Boubakar, Creep behaviour of single hemp fibres. Part I: viscoelastic properties and their scattering under constant climate, J. Mater. Sci. 50 (4) (2015) 1996–2006.
44. Cisse, Ousseynou, Caractérisation du comportement hygro-mécanique des fibres liberiennes élémentaires issues du chanvre, PhD Thesis.
45. Charlet, Karine, Contribution à l' 'etude de composites unidirectionnels renforcés par des fibres de lin : relation entre la microstructure de la fibre et ses proprités m écaniques, PhD Thesis.
46. G. G. Osborne, Micro-Analysis of Textile Fibres: Part IV.-Observations on the Structure of Flax, Manila and Jute, Text. Res. J. 5 (10) (1935) 431–459.

47. P. M. Weaver, The effect of extension/twist anisotropy on compression buckling in cylindrical shells, Compos. Part B Eng. 34 (3) (2003) 251–260.
48. N. J. Pagano, J. C. Halpin, J. M. Whitney, Tension Buckling of Anisotropic Cylinders, in: G. M. L. Gladwell, J. N. Reddy (Eds.), Mech. Composite Materials, Vol. 34, Springer Netherlands, Dordrecht, 1994, pp. 17–30.
49. D. H. Page, F. El-Hosseiny, The mechanical properties of single pulp fibres. Part VI. Fibril angle and the shape of stress-strain curve, J. Pulp Pap. Sci. 84 (1983) TR99—-TR100.